Testing of MM5 System for Application in Taiwan: Prediction of a Cold Air Outbreak Event

Shang-Wu Li[*], Ying-Hwa Kuo[#], and Fang-Ching Chien[*]

[*]Central Weather Bureau

[#]National Center for Atmospheric Research

Abstract

The MM5 is being adapted for operational numerical weather prediction in many countries around the world. It has also been applied to a wide range of research topics, such as explosive cyclones, typhoons, mesoscale convective systems, and air quality studies. In this report, we performed a numerical simulation of a cold air outbreak event which occurred in January 1996 using the MM5. We also compare the performance of 2 experiments, one use the global analysis from ECMWF and the other from the CWB global model to examine the possibility of using the CWB global analysis as MM5's initial data. The results show that MM5 does not perform well in terms of frontal speed when taking the CWB global analysis as model's input. It is however found that adding an objective analysis procedure in the preprocessors does help the simulation.

1. Introduction

The MM5 is a nonhydrostatic, primitive equation model, with many advanced physical parameterization schemes for subgrid-scale cumulus convection, grid-resolvable scale microphysics, planetary boundary layer physics, and atmospheric radiation. Moreover, the MM5 has a very flexible grid-nesting capability, which allows the model to be used with a wide range of grid sizes (e.g., from 1 km to 200 km). Therefore, it is possible to perform nested-grid simulations that resolve synoptic scale systems and cloud-scale systems in the same run. This offers a tremendous amount of flexibility both for research applications and operational numerical weather prediction.

Because of its advanced physics and numerics, the MM5, with more than 300 active users around the world, has been a very popular model in the meteorological community. The MM5 is being adapted for operational NWP in many countries such as Korea, China, Hong Kong, Israel, and Italy. MM5 has also been used at very high-grid resolution to provide operational prediction to guide the operation of field experiments (Kuo et al. 1995). On the research side, MM5 has been used for a wide range of meteorological modeling studies, ranging from explosive cyclones, Mei-Yu fronts, mesoscale convective systems, typhoons, and air quality modeling.

Although the MM5 model has been adapted for various research and operational applications in many parts of the world, setting it up to run effectively in the Taiwan operational NWP environment is not an easy task. For example, the NCEP or ECMWF global analyses which are often used for case studies of historical events are no longer available for operational use in Taiwan. Instead, we have to use CWB global analysis as first guess, in order to run the MM5 system.

In this study, we selected a cold air outbreak event to examine the potential of adapting MM5 for operational application in Taiwan area. Specifically, we first conduct a simulation of a cold air outbreak event using the ECMWF global analysis as the first guess. We then repeat the experiment, but using the CWB global analysis as the first guess. Both of these experiments were conducted with identical physical parameterization.

2. Synoptic description of the event

In this section, we will briefly describe the cold air outbreak event of January 7-8, 1996. At 1200 UTC 7 January, a cyclone of 1015 mb formed over the Sea of Japan (Fig. 1a). A cold front stretched from the center of

the low southwestward into southeastern China. Surface winds behind the cold front were northwesterly. The prefrontal winds were very weak, possibly due to the fact that Wuyi Mountains was located immediately ahead of the cold front, while winds over the Taiwan Straits were predominantly northeasterly.

By 0000 UTC 8 January, the cyclone had deepened to 1000 mb and the cold front had arrived at Taiwan (Fig. 1b). Because of the steep topography of Taiwan, the cold front was not possible to climb up the Central Mountain Range (CMR), and was broken into two parts. The eastern sector had arrived at a location near Hualien. Surface winds behind the cold front were quite strong, generally in the range of 30-40 kts, while ahead of the cold front they were weak northerly or northeasterly. The western portion of the cold front was located over a region of continuous north-to-south pressure gradient. Therefore, both pre-frontal and post-frontal airflow are northerly and northeasterly. With the migration of a strong high pressure system behind the cold front, the pressure gradient was much stronger behind the front.

Upper-level analyses show that a short-wave trough moved eastward from northeastern China to Japan during this time period (not shown). The trough was at a considerable distance away from Taiwan. Figure 2a shows the GMS IR satellite image at 1133 UTC 7 January. At this time, there were no clouds in the vicinity of Taiwan. High cirrus clouds associated with the developing cyclone were visible over the western Sea of Japan. Another region of medium to high clouds was located over the eastern China coast to the north of the cold front. Only scattered shallow clouds existed in the vicinity of the cold front. Therefore, it would have been difficult to define the location of the cold front based on this satellite image alone at this time. To the north of the low-level stratus clouds, there was a narrow region of clear skies immediately off the coast (40°N, 120°E), which suggests that these shallow stratiform clouds formed a few hours after the cold air had moved over the ocean. Apparently, the upward surface fluxes were important for such a modification.

Twelve hours later, mesoscale cellular convection was clearly visible on the GMS IR image at 2333 UTC 7 January (Fig. 2b). High-level cloud mass associated with the developing cyclone had moved over northern Japan. The cloud fields associated with the cold front also show interesting variations. For example, the clouds were relatively shallow over the East China Sea behind the cold front. At the leading edge of the cold front, a rope cloud was clearly evident. The height of the cloud behind the cold front increased progressively toward the low center. Moreover, south to the northeastern China coast, there was a gradual change of cloud fields. Immediately off the coast, the sky was clear, because the fresh cold air did not produce clouds as it rushed off the continent. About 200 km offshore, cellular convection was observed. The size of the cellular clouds become progressively larger and stronger as the air flowed southward. At around 30°N, the cloud fields change into a very different structure, with some deep convection cells embedded within the generally stratiform clouds. Further to the south, there was an area of rope clouds which reflects the leading edge of the cold front. The rope cloud propagated very fast southward, and moved to the southeastern coast by 0333 UTC 8 January (not shown), with a speed of approximately 250 km in 4 hours (17.5 m/s). Cold air damming along the eastern coast of Taiwan may be an important factor that caused the front to move rapidly southward.

3. Model and experiment design

The version of the Penn State/NCAR mesoscale model used in this study is the MM5V2, released in 1996 (Dudhia 1996). The model physics options include: the Kain-Fritsch cumulus parameterization scheme for subgrid-scale convection, Dudhia (1989) simple ice physics, Hong and Pan (1996) PBL scheme, Dudhia (1989) atmospheric radiation scheme, and a 5-layer soil model for ground-temperature calculation (Dudhia 1996). A two-way interactive nested-grid was used with grid sizes of 45 km and 15 km, respectively.

The control experiment (EC00) was initialized at 0000 UTC 7 January 1996, and was performed using all the physics options described above. Initial conditions for the model were obtained from an objective analysis of all the available upper-air and surface observations using the ECMWF global analysis as the first guess. The second experiment (ECNF) is identical to the control

experiment, except that there are no surface energy fluxes.

In order to assess the quality of the CWB global analysis, we performed two other experiments which were initialized only with the global analyses from either the ECMWF (EC-only) or CWB (CWB-only), without enhancement of rawinsonde or surface observations by the Rawins program (which is an objective analysis procedure in the MM5 modeling system).

4. Model results

Twelve hours into the forecast of the EC00 experiment, the cold air has already rushed down to southeastern China (Fig. 3a). The leading edge of the cold air outbreak has reached the northern edge of the Wuyi mountains. Pressure gradients are very large associated with the cold air outbreak, with the cold air moving faster over the ocean than over land.

By 0000 UTC 8 January (Fig. 3b), the cold air has reached northern Taiwan. Sea level pressure pattern shows a mesoscale pressure ridge, which is associated with the cold air damming on the eastern side of CMR. Surface winds near Taiwan are either northerly or northeasterly for both pre-frontal and post-frontal flow, which is not a typical airflow structure of a cold front. The key features differentiating pre- and post-frontal air is wind speed and pressure gradients, which are all much larger in the post-frontal air region than in the prefrontal air region. At the end of the 36-h integration (not shown), the cold air has completely wrapped around Taiwan. An extremely tight pressure gradient (7 mb over a distance of 50 km) is established on the northern edge of the CMR. A well defined pressure ridge is found on the eastern side of Taiwan. Because of the blocking effects of the CMR, winds are very light over most of central, western, and southern Taiwan. It is clear that a well-defined wake zone is established over this region.

Figure 4 shows a cross section that was make along AB of Fig. 3b. Potential temperature field along this cross section shows that the front slopes upward to the north, from 950 mb to 850 mb within a distance of abut 1000 km. Note that the cold air behind the cold front appears to be well mixed. We also note that there is a strong instability within the lowest 25 mb of the PBL, which is an evidence of strong surface energy fluxes near the boundary. As a result of warm sea surface temperature, an unstable lapse rate is created near the ocean surface. Static stability is thus very high at the top of the cold air. Figure 4a also shows that there is a boundary-layer vertical motion jet at the leading edge of the cold front, which is also the region of the rope cloud. It is suggested that the narrow frontal vertical motion is an important factor accounting for the development of the rope cloud. Relative humidity behind the front appears to increase vertically with height (Fig. 4b). A thin layer of high relative humidity (100% or near 100%) is located at the top of the cold air, extending from the northern border of the cross section to a region immediately behind the cold front. It is clear that mixing process has produced clouds at the top of the PBL. Above this PBL top cloud layer, relative humidity is extremely low, implying that the air is of polar origin. We note that there is a zone of moderate to high relative humidity within a width of about 600 km and a depth from the PBL to about 500 mb. This may be the region where the satellite image shows middle clouds with scattered convection. Wind vectors along the cross section also suggest that the polar air appears to be retarded in this region, with possibility of scattered convection suggested by the vertical motion plot.

As discussed earlier, surface energy fluxes may play an important role in this cold air outbreak event, as evident in the development of mesoscale cellular convection behind the cold front that was shown in the satellite images. To examine the role of surface energy fluxes, we performed an experiment with no surface sensible and latent heat fluxes (ECNF), while surface friction is retained. Comparisons between these two experiments (Fig. 5a and Fig. 5b) show that at 0000 UTC 8 January, a sharp cold front is found in the no-flux experiment at a position about 120 km to the south of that in the control experiment. Temperatures between these two experiments differ by more than 10°C behind the cold front, which implies the contribution from surface energy fluxes. Temperature gradients across the cold front are with about the same intensity to the east and the west of Taiwan in EC00. However, they are much stronger to the east of Taiwan than over the Taiwan Strait in the no-flux (ECNF) experiment.

5. Using CWB global analysis

In order to assess the quality of the CWB global analysis, we performed two other experiments which were initialized only with the global analyses from either the ECMWF (EC-only) or CWB (CWB-only), without enhancement of rawinsonde or surface observations by the

Rawins program (which is an objective analysis procedure). It is found that the EC-only experiment performs quite well (Fig. 6a), and the prediction is compatible with that of EC00. However, the CWB-only experiment forecasts a stronger cold front over the East China Sea that moves much slower (Fig. 6b). At 0000 UTC 8 January, the fronts in the EC-only and CWB-only differ by as much as 500 km. This is a fairly large error, suggesting that further improvement of the CWB global analyses is needed.

Another experiment was done in Chien (1998) in an attempt to solve the above problem. Chien (1998) added an objective analysis process in the preprocessors to incorporate observational data into the initial and boundary conditions for the CWB-only experiment. He found that the simulated frontal speed in this experiment agrees well with that of either the EC00 or EC-only experiments.

6. Summary and conclusion

In this study we perform MM5 simulations of a winter-time cold air outbreak event that affects the weather in Taiwan. The purposes of this study are: (1) to test the ability of MM5 at a horizontal resolution of 15 km in simulating this cold air outbreak event, (2) to assess the feasibility of using the CWB global analysis as the first guess for the preparation of MM5 initial condition, and (3) to study the impact of surface energy fluxes on the cold air outbreak. Key findings can be summarized as the following:

The control experiment initialized at 0000 UTC 7 January, using the ECMWF global analysis as the first guess, successfully simulated the cold air outbreak event. The model was able to simulate the development of the rope cloud, the middle-level clouds behind the cold front, and the cold air damming on the eastern coast of Taiwan. The model also simulated mesoscale pressure perturbations caused by the mesoscale mountains over southeastern China.

The surface energy fluxes produced significant modification to the cold air outbreak. Without the surface energy fluxes, the cold air moved much faster southward, and produced a much stronger cold front. In addition, surface energy fluxes are found to be responsible for producing clouds near the top of the PBL.

We also found that the MM5 does not perform well in terms of frontal speed when taking the CWB global analysis as model's input. It is however found in Chien (1998) that adding an objective analysis procedure in the preprocessors does help the simulation. We thus conclude that it is feasible to perform operational MM5 runs in the CWB using the first guess field generated by the CWB global model, with a re-analysis procedure included.

Although fairly good simulation results are obtained in this case study, it is important to bear in mind that this is a winter-time case with strong large-scale forcing. In such a situation, the major forcing (the source of cold air) originates from mainland China where high-density rawinsonde observations can be obtained. In such a situation, the first guess field may not be as important, and one can obtain reasonable good results, as long as the model topography is realistic and the model physics is reasonably good. However, for a summer case, the large-scale forcing is much weaker. Weak forcing responsible for convection can originate over the data void region like oceans. As a result, the model may be much more sensitive to the analysis over the ocean. In such situation, the quality of the first guess can become critical.

Acknowledgment

The numerical experiments presented in this report were performed by Dr. Wei Wang. The satellite pictures were provided by Ms. Chen-Wen Wu at the CWB Satellite Center. Their assistance is greatly appreciated.

References

Chien, F.-C., 1998: Precipitation forecasts of the MM5. *天氣分析與預報研討會氣象論文彙編(87)*。

Dudhia, J., 1989: Numerical study of convection observed during the Winter Monsoon Experiment using a mesoscale two-dimensional model. *J. Atmos. Sci.*, **46**, 3077-3107.

Dudhia, J., 1996: Whats new in MM5 version 2. *Preprints, 6th PSU/NCAR Mesoscale Model Users Workshop.* 22-24 July 1996, Boulder, CO, 1-3.

Dudhia, J., 1996: A multi-layer soil temperature model for MM5. *Preprints, 6th PSU/NCAR Mesoscale Model Users Workshop.* 22-24 July 1996, Boulder, CO, 49-50.

Hong, S. Y., and Pan, H.-L., 1996: Nonlocal boundary layer vertical diffusion in a medium-range forecast model. *Mon. Wea. Rev.*, **124**, 2322-2339.

Kuo, Y.-H., K. Gao, and S. Low-Nam, 1995: Verification of MM4, NGM and ETA prediction during STORM-FEST. *NCAR manuscripts.* 55pp.

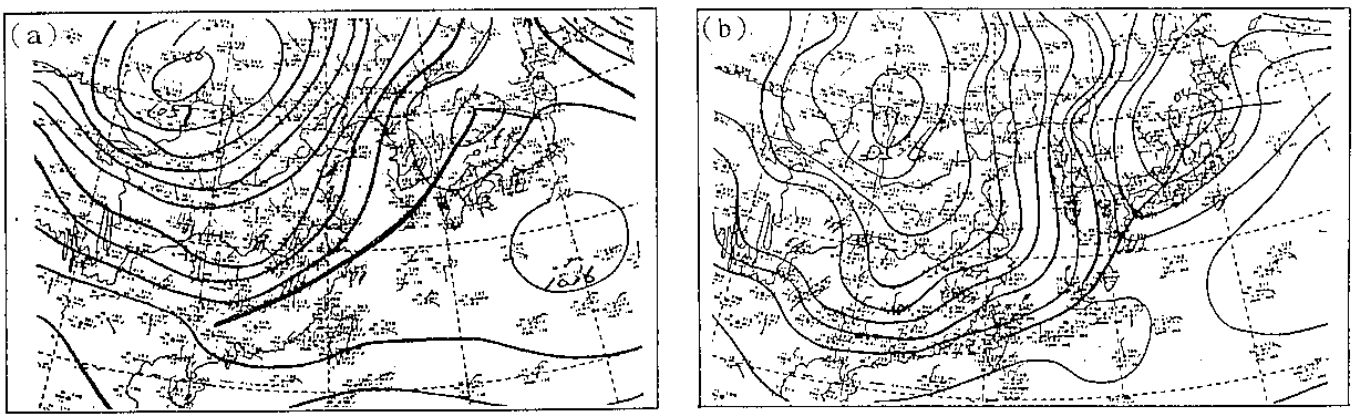

Fig. 1. Surface analyses at (a) 1200 UTC 7, and (b) 0000 UTC 8 January 1996.

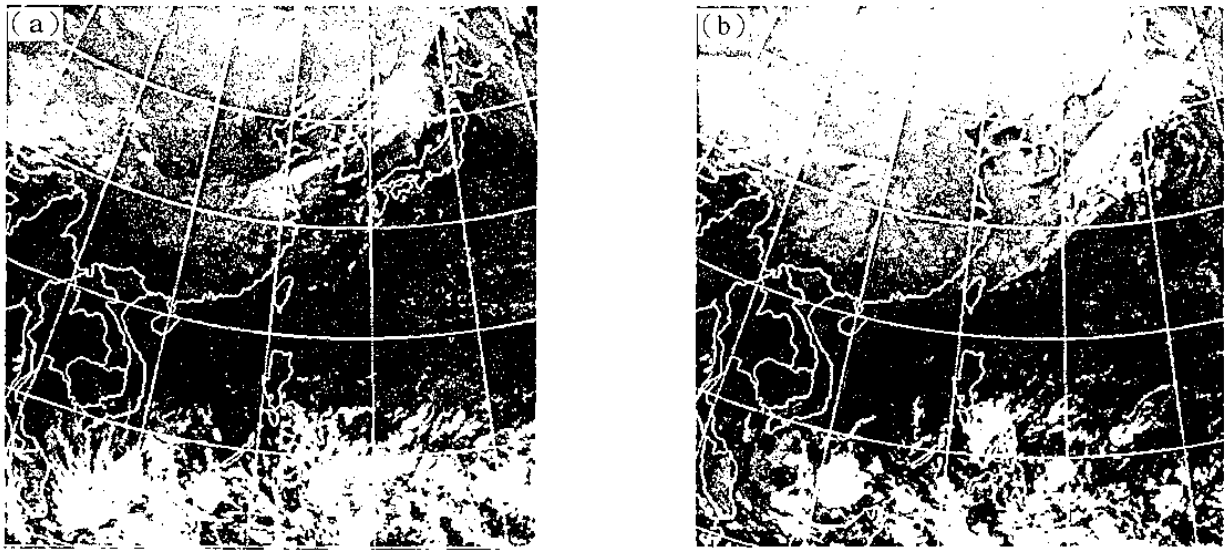

Fig. 2. IR satellite picture at (a) 1133 UTC 7 January and (b) 2333 UTC 7 January 1996.

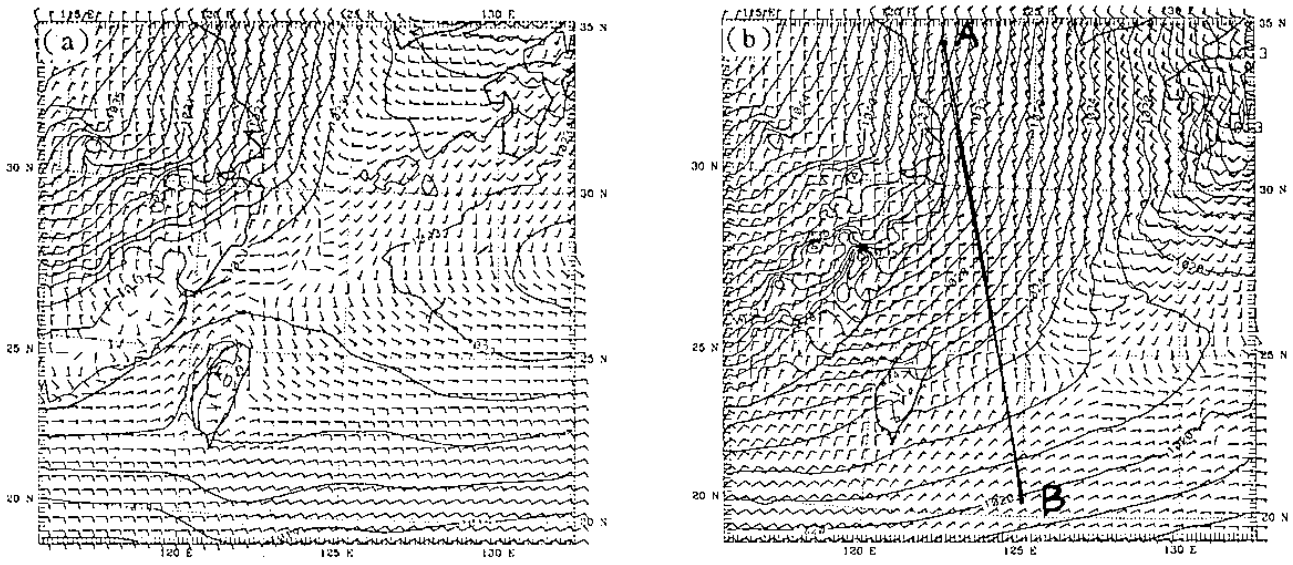

Fig. 3. Simulated sea level pressure and surface wind at (a) 1200 UTC 7, and (b) 0000 UTC 8 January 1996 for the EC00 experiment.

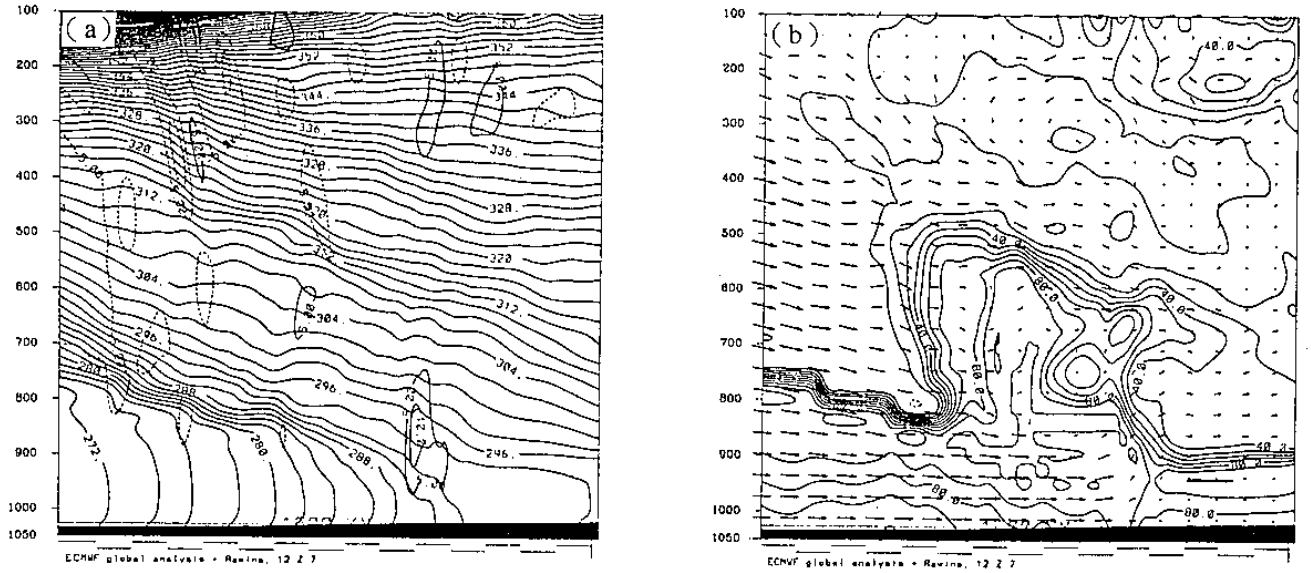

Fig. 4. Vertical cross sections of (a) potential temperature (solid line) and vertical motion (thin solid and dashed lines), and (b) relative humidity (solid lines) and two-dimensional wind vectors along the cross section.

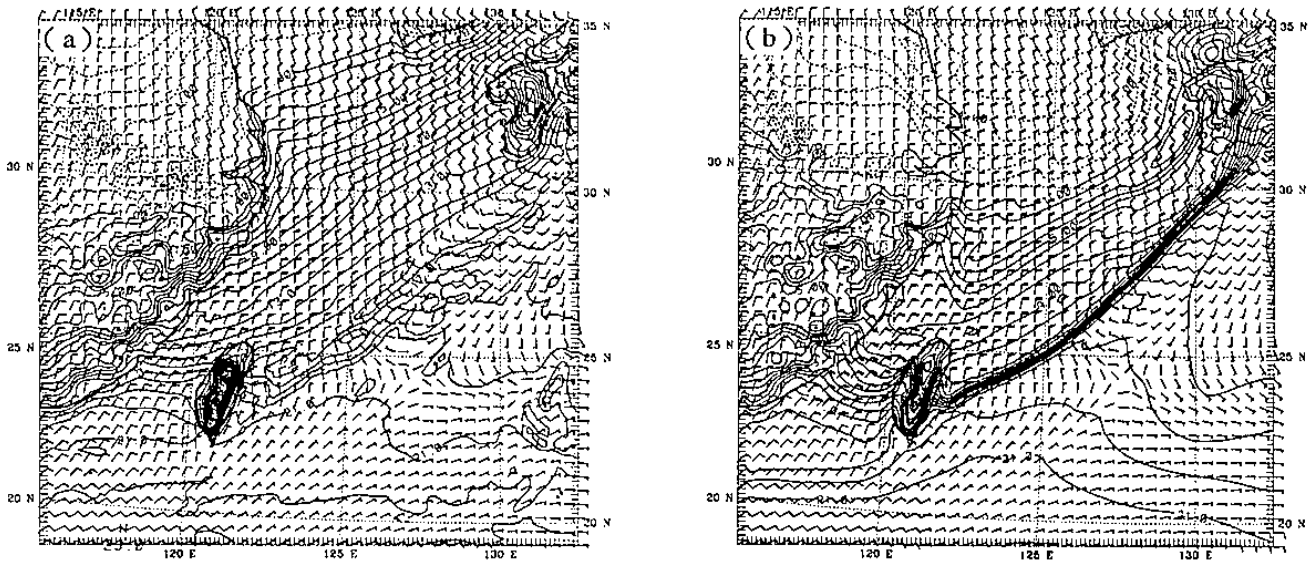

Fig. 5. Surface temperature prediction verifying at 0000 UTC 8 for (a) EC00, and (b) for ECNF.

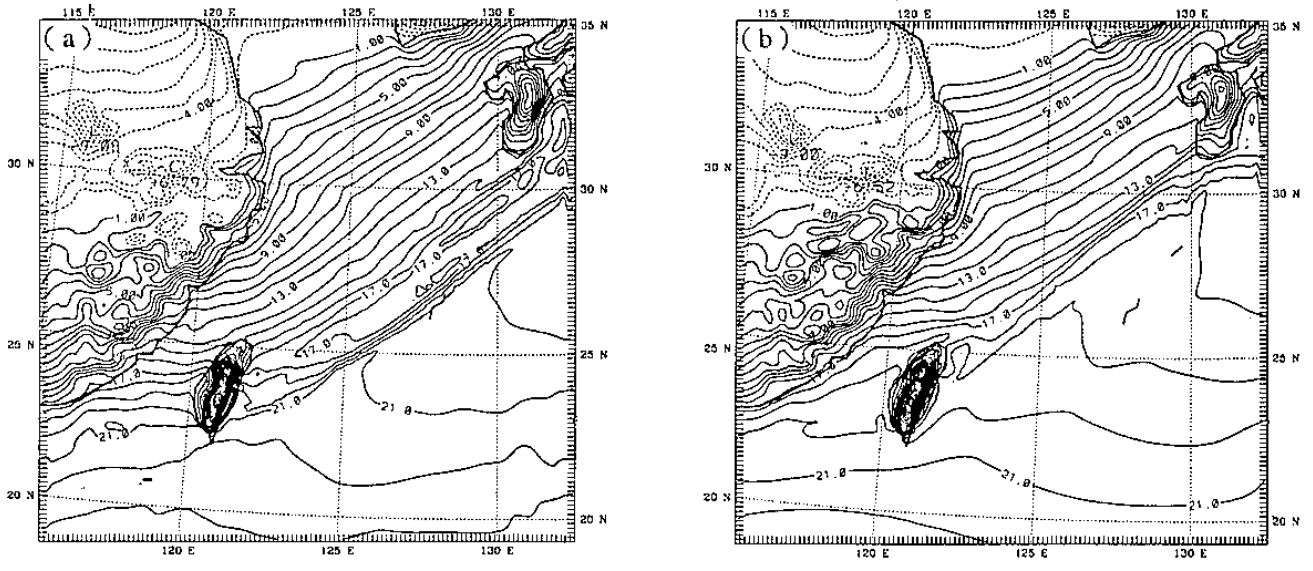

Fig. 6. Twelve hour prediction of surface temperature for (a) the EC-only experiment, and (b) the CWB-only experiment.